On the interpretation of Langmuir probe data inside a spacecraft sheath

J. Olson,[1] N. Brenning,[1] J.-E. Wahlund,[2] and H. Gunell[3]
[1]*Space and Plasma Physics, Royal Institute of Technology (KTH), Teknikringen 31, SE-10044 Stockholm, Sweden*
[2]*Swedish Institute of Space Physics, Box 537, SE-751 21 Uppsala, Sweden*
[3]*Belgian Institute for Space Aeronomy, Avenue Circulaire 3, B-1180 Brussels, Belgium*

(Received 16 April 2010; accepted 2 August 2010; published online 19 October 2010)

If a Langmuir probe is located inside the sheath of a negatively charged spacecraft, there is a risk that the probe characteristic is modified compared to that of a free probe in the ambient plasma. We have studied this probe-in-spacecraft-sheath problem in the parameter range of a small Langmuir probe (with radius $r_{LP} \ll \lambda_D$) using a modified version of the orbit motion limited (OML) probe theory. We find that the ambient electron contribution $I_e(U_{LP})$ to the probe characteristic is suitably analyzed in terms of three regions of applied probe potential U_{LP}. In region I, where the probe is negatively charged (i.e., $U_{LP} < U_1$, where U_1 is the potential in the sheath at the probe position), the probe characteristic $I_e(U_{LP})$ is close to that of OML theory for a free probe in the ambient plasma. In the probe potential range $U_{LP} > U_1$, there is first a *transition region* II in applied potential, $U_1 < U_{LP} < U_2$, in which the key factor to determine the shape of $I_e(U_{LP})$ is a potential minimum U_M between the probe and the ambient plasma. This minimum gives the depth $U_{pl} - U_M$ of a potential barrier that prevents the lowest energy ambient electrons from reaching the probe. For a high enough positive probe potential, in region III, the barrier becomes small. Here, $I_e(U_{LP})$ again approaches OML theory for a free probe. The boundary U_2 between regions II and III is somewhat arbitrary; we propose a condition on the barrier, $U_{pl} - U_M \ll k_B T_e / e$, as the definition of region III. The main findings in this work are qualitative rather than quantitative. The existence of the transition region points to that special care must be taken to extract plasma parameters from measured $I(U_{LP})$ as the probe characteristic is likely to depart from usual OML in crucial respects: (1) the ambient plasma potential U_{pl} falls into the transition region, but there is no obvious knee or other feature to identify it, (2) there is in this region no exponential part of $I_e(U_{LP})$ that can be used to obtain T_e, instead, (3) the probe size is important in determining the curve shape. We have tentatively applied our simplified probe-in-sheath model to real probe data from the Cassini spacecraft, taken in the dense plasma of Saturn's magnetosphere. We propose that our model gives a better description than OML of measured Langmuir probe sweeps in space plasmas where the Langmuir probe is situated within the spacecraft sheath, i.e., for long Debye lengths. The understanding of these probe sweep effects in such regions may improve by self-consistent particle simulations of the spacecraft environment. © *2010 American Institute of Physics.* [doi:10.1063/1.3482155]

I. INTRODUCTION

We consider the evaluation of ambient plasma parameters, such as potential U_{pl}, electron density n_{e0}, and electron temperature T_e, from spacecraft Langmuir probe data. With spinning spacecrafts, probes in the spin plane can be put outside the spacecraft sheath by using centrifugally stretched wire booms of sufficient length $\ell_{boom} \gg \lambda_D$ or $\ell_{boom} \gg r_{SC}$, where λ_D is the Debye length of the ambient plasma and r_{SC} is a characteristic radius of the spacecraft, so that either the probe is Debye screened from the spacecraft, or the spacecraft is small enough not to have a long-range influence anyway. If the boom is short, as may become the case when the probe is mounted on a three-axis stabilized platform, the probe may in certain cases be found within the spacecraft sheath. The local potential at the probe position, which we denote by U_1, will differ then from the ambient plasma potential U_{pl}. We use a simplified geometrical model to illustrate how the potential structure in the spacecraft-and-probe system depends on the potentials of spacecraft and probe and on the length scales involved, and present an analytical model for a first-order estimate of the ambient electron collection $I_e(U_{LP})$ in the same geometry. We assume the parameter regime of collision-free plasmas and small probes (with radius $r_{LP} \ll \lambda_D$) and use a modified version of the orbit motion limited (OML) probe theory for electron collection. The main findings are qualitative rather than quantitative. The existence of a *transition region* above U_1 points to that special care must be taken to extract plasma parameters from measured $I(U_{LP})$ as this curve likely departs from usual OML theory in important respects: (1) the ambient plasma potential U_{pl} has no obvious knee or other feature to identify it, (2) there is above U_1 no exponential part of $I_e(U_{LP})$ that can be used to obtain T_e, instead, (3) the curve shape depends strongly on the probe size in a way that, for reliable quantitative evaluation, must be separated from the dependencies

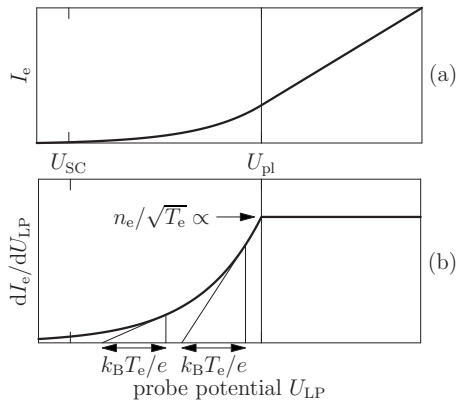

FIG. 1. An illustration of how plasma parameters are obtained from a measured probe characteristic in OML theory. (a) The ambient electron collection current I_e as a function of the potential U_{LP} of a small, spherical probe in a collisionless plasma where OML theory [Eq. (1)] applies. If $r_{LP} \ll \lambda_D$ is not satisfied, one should expect a reduction in current for highly positive probe potentials, as the collection radius becomes comparable to λ_D. (b) The relation between features in the dI_e/dU_{LP} curve and the plasma parameters. The *shape* of the exponential part of the curve (where $U_{LP} < U_{pl}$) gives the electron temperature T_e, the *potential* at the knee gives the plasma potential U_{pl}, and the *level* at the knee gives the combined parameter $n_e/\sqrt{T_e}$. If any of these three features becomes uncertain, the determination of plasma parameters also becomes uncertain in the absence of other experimental information such as ion density derived from the Langmuir probe sweep or electron density determined from upper hybrid emission.

on n_{e0} and T_e. The paper is organized as follows. In Sec. II we summarize for reference how plasma parameters U_{pl}, n_e, and T_e are extracted from Langmuir probe characteristics $I_e(U_{LP})$ in standard OML theory, and in Sec. III we discuss the effect that arises when the probe is in the spacecraft sheath. Section IV describes a simplified model to deal with that problem, and in Sec. V a comparison is made between that model's predictions and real space data. Section VI finally contains a summary and discussion.

II. DERIVATION OF PLASMA PARAMETERS FROM PROBE CHARACTERISTICS

Figure 1(a) shows the electron current to a spherical Langmuir probe, with a small radius $r_{LP} \ll \lambda_D$, in a homogeneous and collisionless plasma. In this parameter regime, the OML theory applies and the probe characteristic[1,2] is given by

$$I_e(U_{LP}) = \sqrt{8\pi} r_{LP}^2 n_{e0} e \sqrt{\frac{k_B T_e}{m_e}} e^{e(U_{LP}-U_{pl})/(k_B T_e)} \quad \text{when } U_{LP} < U_{pl},$$

$$I_e(U_{LP}) = \sqrt{8\pi} r_{LP}^2 n_{e0} e \sqrt{\frac{k_B T_e}{m_e}} \left(1 + \frac{e(U_{LP}-U_{pl})}{k_B T_e}\right) \quad \text{when } U_{LP} > U_{pl}. \tag{1}$$

The OML theory needs modification when the area influenced by the probe, including the sheath around it, is not sufficiently small compared to the Debye length.[3] In the present study we disregard such effects.

The desired plasma parameters we will discuss in this work are the ambient plasma potential U_{pl}, the electron density n_{e0}, and the electron temperature T_e. These are obtained in OML theory as the combination of (U_{pl}, n_{e0}, T_e) in Eq. (1) that gives the best fit, according to some suitable criterion, to a measured probe characteristic $I(U_{LP})$, with due consideration of contributions to the probe current other than ambient electrons. Although such fits might deal exclusively with the $I(U_{LP})$ curve, it is important to realize that information-carrying features of the probe characteristic are more clearly seen in the derivative dI/dU_{LP}, as illustrated in Fig. 1(b): (1) the *slope* of each individual part of the curve for $U_{LP} < U_{pl}$ can in principle give T_e, (2) the location of the *knee* in the derivative gives U_{pl}, and (3) the *value* of the derivative at the knee gives the combined quantity $n_{e0}/\sqrt{T_e}$. The coupling between these three features in the dI_e/dU_{LP} curve and the plasma parameters is fundamental. We propose that, if they are uncertain or ambiguous in a measured probe characteristic, it is difficult to find an objective criterion to define the best fit of Eq. (1).

III. POTENTIAL STRUCTURE AROUND A BIASED LANGMUIR PROBE IN A SHEATH

To bring forth the main features, we use a simplified geometry: a spherical spacecraft of radius r_{SC}, with a spherical probe with radius r_{LP} at a distance ℓ_{boom} from the spacecraft surface. We disregard (1) the influence on the potential by the probe boom, (2) wake effects, (3) the depletion of particles in the sheath due to absorption on the spacecraft, and the probe. The potential is under these approximations the same as that from two screened point charges. For example, the undisturbed potential U_1 at the probe position is found from the potential field $U(r)$ around single point charge q, representing the spacecraft,

$$U(r) - U_{pl} = \frac{q}{4\pi\varepsilon_0} \frac{1}{r} e^{-r/\lambda_D}, \tag{2}$$

with the charge q chosen such that at the spacecraft radius, $r = r_{SC}$, $U(r)$ coincides with the specified spacecraft potential U_{SC},

$$U_{SC} - U_{pl} = U(r_{SC}) - U_{pl} = \frac{q}{4\pi\varepsilon_0} \frac{1}{r_{SC}} e^{-r_{SC}/\lambda_D}, \tag{3}$$

so that $U(r)$ can be expressed in terms of U_{SC} instead of q,

$$\frac{U(r) - U_{pl}}{U_{SC} - U_{pl}} = \frac{r_{SC}}{r} \frac{e^{-r/\lambda_D}}{e^{-r_{SC}/\lambda_D}} = \frac{r_{SC}}{r} e^{-(r-r_{SC})/\lambda_D}. \tag{4}$$

The sought potential U_1 is now simply $U(r)$, evaluated at the probe position $r = r_{SC} + \ell_{boom}$,

$$U_1 = U(r_{SC} + \ell_{boom}) = U_{pl} + (U_{SC} - U_{pl}) \frac{r_{SC}}{r_{SC} + \ell_{boom}} e^{-\ell_{boom}/\lambda_D}. \tag{5}$$

Figure 2 shows the potential structure around a negatively charged spacecraft as we will consider here, and defines the variables to be used in this work. The key feature in Fig. 2 is a potential minimum U_M (at the X-point of the equipotential curves) that arises for positively charged probes, i.e., when $U_{LP} > U_1$. The electron collection current $I_e(U_{LP})$ will depend on the depth and shape of this minimum, since it acts as a barrier and prevents all ambient electrons with energy be-

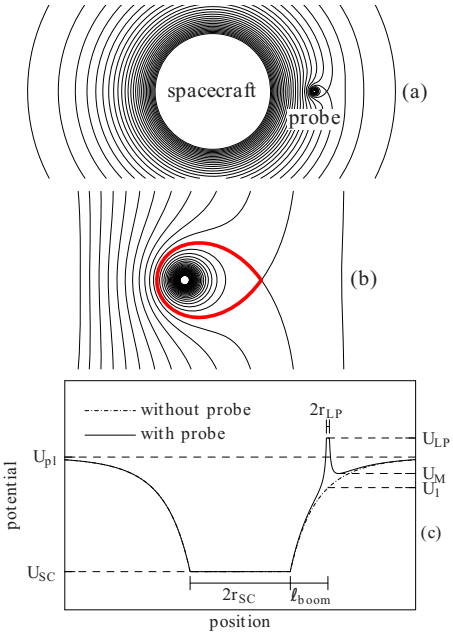

FIG. 2. (Color online) The potential structure in a simplified spacecraft-and-probe geometry and definitions of the parameters U_{SC}, U_{LP}, U_{pl}, U_1, U_M, r_{SC}, r_{LP}, and ℓ_{boom} to be used in this work. (a) Lines of constant potential around a negative spacecraft and a probe with a potential that is more positive than its surroundings. The probe in this figure thus attracts electrons. (b) Detail of the same potential structure as in (a), in the area around the probe. (c) The same potential as in (a), evaluated along the common axis of the spacecraft and the probe. The potential U_1 is the potential that would be found at the center of the probe position, if the probe was removed and only the spacecraft remained. A potential minimum, denoted U_M, acts as a barrier that keeps the lowest energy ambient electrons from reaching the probe. This reduces the electron collection current below that of a free probe, held at the same potential in the ambient plasma.

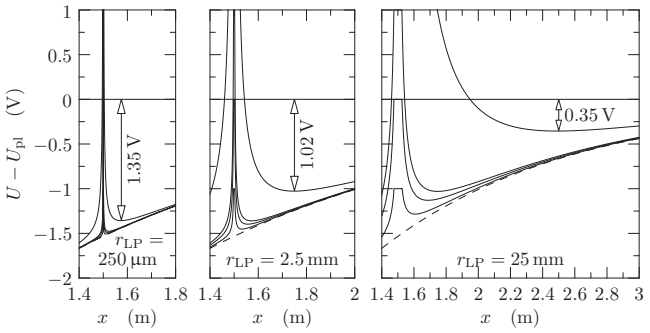

FIG. 3. A demonstration of how the depth of the potential minimum U_M depends on variations in the probe radius r_{LP}, with x being the distance from the spacecraft center. The parameters T_e, n_e, λ_D, r_{SC}, and ℓ_{boom} are those of the Cassini standard case in Table I. The figures show potential profiles [of the same kind as in Fig. 2(c)] near the probe for varied applied probe potentials U_{LP}. In the case of a very small probe, with its small region of influence, the potential minimum changes only marginally with the probe bias. A smaller probe, therefore, to a larger extent experiences only the local potential U_1 and local, reduced density n_{e1}. In the case of the largest probe (with r_{LP}=25 mm as in the Cassini standard case), the potential barrier almost disappears for the highest applied probe potential $U_{LP}=U_{SC}+30$ V, and the probe becomes much more exposed to the ambient plasma.

low $e|U_M-U_{pl}|$ from reaching the probe. The complications are two: first, the depth and spatial width of the minimum depend both on the potential differences $U_{SC}-U_{pl}$, U_1-U_{pl}, $U_{LP}-U_{pl}$, and the involved scale lengths λ_D, r_{SC}, ℓ_{boom}, and r_{LP}. Second, in this asymmetric potential structure, both the ambient electrons' entry through the barrier and their collection at the probe are complicated problems, probably not tractable analytically, especially not for realistic spacecraft geometries.

Let us first look at the dependence of the potential minimum on the probe radius r_{LP}. It is illustrated in Fig. 3 which shows the radial potential profiles close to the probe for a reference case, with the parameters chosen to be relevant for the Cassini probe data to be presented in Sec. V. These parameters are referred to as the *Cassini standard case* in Table I. Apart from the actual Cassini probe size, r_{LP}=25 mm, Fig. 3 also shows the situation with two smaller probes. The key feature in these curves is the potential barrier $|U_M-U_{pl}|$ against ambient electrons. Although all three probes apparently are small compared to other involved dimensions, obeying $r_{LP} \leq 25$ mm $\ll \min(\ell_{boom}, \lambda_D) = \lambda_D \approx 1.3$ m, the barrier varies considerably with the probe size. For example, the uppermost curve in each panel of Fig. 3 shows the potential profiles for the same applied probe potential $U_{LP}-U_{pl}$=30 V. At this potential, the barrier is 1.35 V for the smallest probe, and rejects a large part of the ambient electrons, while the barrier for the real-sized 25 mm probe is only 0.35 V and lets most of them in. The origin of this strong dependence on probe size, even well within the regime of $r_{LP} \ll \lambda_D$, lies in that for a fixed probe potential, the probe carries a charge that is proportional to r_{LP}. So does, for example, the probe charge in Fig. 3 increase tenfold for each tenfold increase of r_{LP}. Due to its stronger charge, a larger probe thus has a greater influence over the potential field and over a larger region, pulling the minimum potential toward zero and pushing its location outward. Similar to the spacecraft, the probe contribution to the potential field is $(U_{LP}-U_1)(r_{LP}/r)\exp(-(r-r_{LP})/\lambda_D)$, where r is the distance from the probe center. Here, the discussed size scaling is evident in the factor r_{LP}/r and it is also clear that not even an infinite λ_D will eliminate this effect.

We can, based on Figs. 3 and 4, make a first qualitative discussion of the probe-in-sheath effects on the information-carrying features in the derivative dI_e/dU_{LP} of the characteristics. Consider first probes that are held at, and below, the local potential U_1. In this range of U_{LP}, there is no minimum, and the potential is monotonically decreasing from the ambient plasma to the probe. Since a Maxwell distribution retains its shape in a repulsive potential, although its density is

TABLE I. Real parameters for the Cassini mission and those used in the "Cassini standard case" for calculating the curves in Figs. 3, 4, and 6. Probe radius and boom length are found in the instrument description (Ref. 4) and plasma parameters (temperature, density, and Debye length) are taken from Ref. 5.

	Real Cassini parameters	Cassini standard case
r_{LP}	25 mm	25 mm
ℓ_{boom}	1.5 m	1.5 m
Spacecraft size	Irregular	r_{SC}=8 m, to match simul.
K_{float}	2.3–3.1, from simul.	2.5
$k_B T_e$	0.5–7 eV	2.2 eV
n_e	5×10^6 to 1.5×10^8 m^{-3}	7×10^7 m^{-3}
λ_D	400 mm–9 m	1.31 m

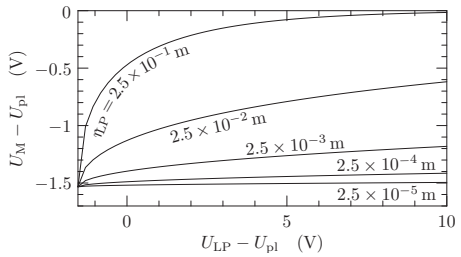

FIG. 4. The potential barrier $U_M - U_{pl}$ as a function of the probe potential, for the Cassini standard case of Table I, but with different probe sizes. Consider the curve with the real Cassini probe radius $r_{LP}=2.5\times10^{-2}$ mm, when it is held around the ambient plasma potential, i.e., where $U_{LP}-U_{pl}=0$. For a free probe in the ambient plasma, we here expect an identifiable transition feature in the probe characteristic, as shown in Fig. 1(b). The physical reason is that here the probe changes from attractive to repulsive when U_{LP} goes below U_{pl}. In the corresponding curve (third from the top in the rightmost panel of Fig. 3), we see that the probe is still attractive with respect to its immediate surroundings. The electron collection is instead to a large extent governed by the potential barrier shown above. It varies smoothly with U_{LP} and there is no reason to expect any transition feature at the plasma potential.

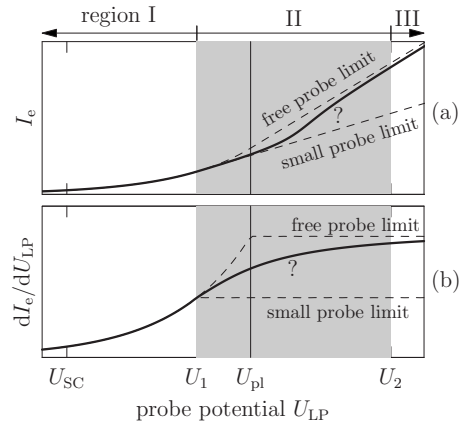

FIG. 5. (a) A qualitative illustration of the expected ambient electron current $I_e(U_{LP})$ to a probe in the sheath of a spacecraft. The undisturbed potential at the probe U_1 lies between the spacecraft potential U_{SC} and the ambient plasma potential U_{pl}. The $I_e(U_{LP})$ curve is bounded by an upper limit corresponding to a free probe in the ambient plasma, and by an approximate lower limit corresponding to a very small probe at the real probe position. For a probe that is more negative than its surroundings, i.e., $U_{LP}<U_1$, these upper and lower bounds coincide, and the standard OML theory for a repulsive probe should be possible to use. In the positive-bias extreme, there should be a potential $U_{LP}=U_2$ above which the probe becomes effectively exposed to the ambient plasma and standard OML is again applicable. Probe-in-sheath effects are therefore expected only in a transition region between U_1 and U_2. (b) A qualitative illustration of the expected derivative of the current. A comparison to Fig. 1 shows that key information-bearing features of the characteristics are found in the transition region and can be severely influenced. This region is therefore shaded here.

scaled down, the probe should here experience electrons with the ambient temperature T_e and density $n_{e1}=n_{e0}e^{-(U_1-U_{pl})/(k_BT_e)}$, yielding the OML current with this temperature and density. Note that since the relevant potential difference to use in the OML model here is $U_{LP}-U_1$, this current is the same as that of a free probe in the ambient plasma, i.e., given by Eq. (1) (we here neglect that a fraction of electrons, of the order of $\sqrt{m_e/m_i}$, have overcome the repulsive potential and hit the spacecraft and are therefore missing). Let us call this *region I* of the probe sweep. Next, let us consider the other extreme, probes held at high positive potential. For a probe with radius 25 mm, we saw in Fig. 3 that the barrier becomes only 0.35 V at 30 V positive probe bias. Figure 4 shows a more systematic overview of the dependence of $U_M(U_{LP})$ on probe size, still for the reference case. For a big probe with 250 mm radius, the barrier would practically disappear $(U_{pl}-U_M \ll k_BT_e/e)$ for $U_{LP}-U_{pl}$ above a few volts. Such a disappearance of the barrier means that the probe becomes exposed to the ambient plasma and, as in region I, the probe characteristics should approach that of a free probe. Let us call the range of high positive potentials in which this happens *region III* and define the potential U_2 as its beginning. The situation can thus be summarized as follows (see Fig. 5): below the local potential in the sheath U_1, and also above a potential U_2 that depends on probe size, one can expect the standard OML theory of Eq. (1) to hold at least approximately. In a transition region II between these, one can expect the current to be reduced below the OML value. In this transition region, there is an upper limit given by OML theory and an approximate lower limit corresponding to a very small probe. The characteristics in the extreme small probe limit consist of only regions I and II, and the whole sweep is close to OML theory for a probe sampling the local parameters U_1, n_{e1}, and T_e at the probe position (only below U_1 does this give the same functional dependence as a probe sampling the ambient U_{pl}, n_{e0}, and T_e). For such a probe sweep, the ambient U_{pl} and n_{e0} cannot be obtained without additional modeling. Finally, for finite-size probes, the shape of the curve in the transition region II depends on probe size in a way that departs from OML theory. A comparison between Figs. 5(b) and 1(b) shows that this could be a problem. In this region, two out of three key features for evaluation of plasma parameters are found, namely the slope and the position of the knee.

IV. A SIMPLE ANALYTICAL PROBE-IN-SHEATH MODEL

We here seek the ambient electron contribution to the probe current in region II as a function of the applied bias relative to the spacecraft, $I_e(U_{LP}-U_{SC})$. Let us make a thought experiment where we follow the time evolution of a situation where there are initially no electrons in the region enclosed by the thick curve in Fig. 2(b). Along this curve (or surface, in three dimensions), the potential is the same as that of the potential barrier at the *X*-point and this is the most negative potential that completely encloses the probe. We will call this surface the *X-surface*. Consider replacing the real probe with a point charge, placed at the probe center and of strength such that the potential outside the real probe's surface is unchanged. The inflow of electrons from the ambient plasma through the *X*-surface will be the same as it was with the real probe. Let us call this electron current $I_{e,in}$. The electrons that have crossed the barrier will move about inside the potential trap around the point charge, but since it absorbs no electrons, none will be lost. There will eventually be an equilibrium in electron flow, where an equal number of electrons exit to the ambient plasma through the *X*-surface, i.e., $I_{e,out}=I_{e,in}$. Consider now, in this steady state situation, the electron density at the *X*-surface. All electrons at the *X*-surface have followed dynamical trajectories from the am-

bient plasma. According to Liouville's theorem,[6] the phase space density is constant along such trajectories. At equilibrium, we therefore propose that the electron density at the *X*-surface is the ambient plasma density reduced by a Boltzmann factor,

$$n_{e,X\text{-surface}} = n_{e0} e^{-e(U_M - U_{pl})/k_B T_e}. \quad (6)$$

The next step in this thought experiment is to replace the point charge with a probe that is so small that it collects a negligible current in the sense $I_{LP} \ll I_{e,in}$. The collection of such a small current should have negligible influence on the equilibrium state. The *X*-surface, with an electron density given by Eq. (6), can then be regarded as a *source region* for the electron current drawn by this small probe.

Finally, we switch to a real probe with finite radius, and make two admittedly crude approximations in order to formulate an analytical solution. First, we assume that, also for a finite-size probe, $I_{LP} \ll I_{e,in}$ holds and Eq. (6) gives the electron density at the *X*-surface. Second, we approximate the current drawn by the probe from the *X*-surface by that drawn from a homogeneous infinite plasma with density $n_e = n_{e,X-surface}$ and potential $U_{pl} = U_{X-surface} = U_M$. With these approximations being made, we can formulate a model intended to capture the qualitative features of the probe-in-sheath effects. Our method is a recipe in five steps for calculating the electron current $I_e(U_{LP})$ to a probe, for a given satellite-and-probe geometry, and assumed ambient plasma U_{pl}, n_{e0}, and T_e:

(1) Choose the real probe radius r_{LP} and boom length ℓ_{boom}, and a suitable value of the spacecraft radius r_{SC}.
(2) Choose the spacecraft floating potential as $U_{SC} = -K_{float} k_B T_e / e$. The constant K_{float} has to be separately assessed, including, for example, photoelectron current and ion current (see Sec. V).
(3) Obtain λ_D from n_{e0} and T_e and use Eq. (5) to obtain the potential U_1 at the probe position in the sheath.
(4) For $U_{LP} > U_1$, obtain the potential U_M as a function of U_{LP} from calculated radial profiles such as in Fig. 2(c).
(5) The probe-in-sheath model is obtained by modifying the OML equations so that the attractive-probe region begins at U_1 instead of U_{pl}. In this attractive region where $U_{LP} > U_1$, the source plasma density is $n_{e,X-surface}$ from Eq. (6) and the probe potential is compared to the *X*-surface potential U_M,

$$I_e(U_{LP}) = \sqrt{8\pi} r_{LP}^2 n_{e0} e \sqrt{\frac{k_B T_e}{m_e}} e^{e(U_{LP} - U_{pl})/(k_B T_e)} \quad \text{when } U_{LP} < U_1,$$

$$I_e(U_{LP}) = \sqrt{8\pi} r_{LP}^2 n_{e0} e^{-e(U_M - U_{pl})/(k_B T_e)} e \sqrt{\frac{k_B T_e}{m_e}} \times \left(1 + \frac{e(U_{LP} - U_M)}{k_B T_e}\right) \quad \text{when } U_{LP} > U_1. \quad (7)$$

As seen in Eq. (7), for $U_{LP} < U_1$, the usual OML model is retrieved. For $U_{LP} > U_1$ on the other hand, the proposed model deviates from OML in that it compares the probe potential to U_M, rather than to the background plasma potential, and in that it rescales the density with a Boltzmann factor $e^{-e(U_M - U_{pl})/(k_B T_e)}$. Furthermore, the potential minimum U_M, and therefore also the density rescaling, are themselves functions of the probe potential. Thus, when the probe is in the sheath [approximately when $|U_1 - U_{pl}|/(k_B T_e/e) > 0.2$], the $I_e(U_{LP})$ curves according to this model are found to depend, through U_M, on all geometry parameters λ_D, r_{SC}, r_{LP}, and ℓ_{boom}. These dependencies need to be understood and decoupled from the influence of the ambient parameters U_{pl}, n_{e0}, and T_e that are to be measured. The dependence on r_{LP} is the most significant and illustrated in Fig. 6 by a set of dI_e/dU_{LP} curves that are obtained from Eq. (7) for the reference case plasma parameters, and with varied probe radius (the same values of r_{LP} as in Fig. 4). These show all the features proposed based on general arguments in Fig. 2. The extent of the transition region and the curve shape within it depends on all the geometry factors and departs fundamentally from OML theory in several respects: (1) although the ambient plasma potential U_{pl} falls here, there is no knee or other obvious way to identify it, (2) there is no exponential part of $I_e(U_{LP})$ that can be used to obtain T_e, and (3) the curve shape depends on the probe size r_{LP}. In particular, the slope dI_e/dU_{LP}, which is essential for the estimate of T_e, decreases with decreasing probe size r_{LP}. Standard OML analysis, by fitting an exponential to a part of measured $I_e(U_{LP})$ curves, could therefore overestimate the electron temperature.

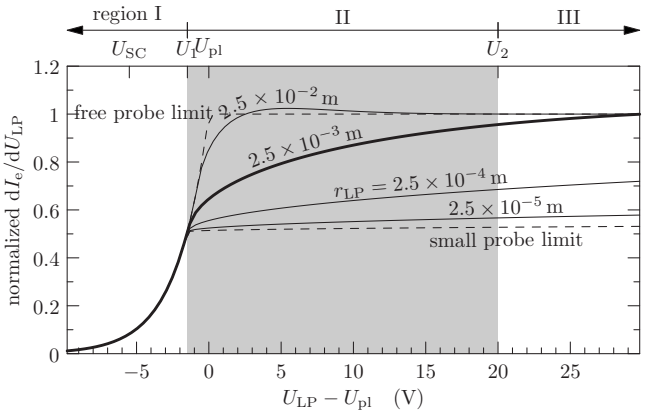

FIG. 6. A demonstration of the sensitivity of the probe-in-sheath model to variations in the probe radius r_{LP}. The graph shows curves of dI_e/dU_{LP}, obtained by the probe-in-sheath model of Eq. (7). The probe radius is varied, but the rest of the parameters are, for all curves, those of the Cassini standard case of Table I. To enable comparison between these characteristics, which correspond to probes with very different cross sections, the curves are normalized by $r_{LP}^2 n_{e0} e\sqrt{8\pi/(m_e k_B T_e)}$ so that they all tend toward the same plateau. As in Fig. 5, the dashed curves denote the free probe limit and the small probe limit. The potentials at the top of the figure (U_{SC}) mark where the probe attains these potentials. The shaded area, from U_1 to U_2, shows the proposed transition region for the real Cassini probe radius, 25 mm.

V. COMPARISON WITH CASSINI SPACECRAFT DATA

For comparison with real data we have selected an often occurring sweep type as measured by the Langmuir probe[4] on the Cassini spacecraft. This particular sweep was taken at 14 July 2005, 20:09:18, from the inner magnetosphere (plasma disk) of Saturn,[5] where the plasma density is high so that the electron saturation current exceeds the photoemission current, and the probe acquires a negative floating po-

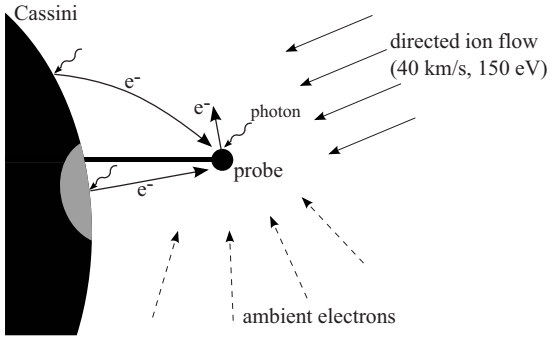

FIG. 7. Five types of current that can contribute to the probe characteristics in the Cassini data: (1) ambient electrons, (2) ions with mainly a directed speed (due to corotation with Saturn and spacecraft motion), (3) photoelectrons from the probe, and (4) photoelectrons from the spacecraft. The latter are divided into two categories: (4a) those that originate from the photoelectron footpoint (indicated by a grey area) from which the photoelectrons can hit an unbiased probe and (4b) those originating outside the photoelectron footpoint and that can reach the probe only when it is biased positive, $U_{LP} > U_1$. (This photoelectron footpoint should not be considered as an area with a sharp boundary. Photoelectrons are emitted from the surface with a spread in energy and in directions at all angles to the surface. From each point some will be directed sideways toward the probe and some away. The potential difference of $U_{SC} - U_1$ compared to $k_B T_{photo}/e$ also influences the process. However, if it is regarded as an area with a diffuse and gradual boundary, the concept of a photoelectron footpoint is useful.)

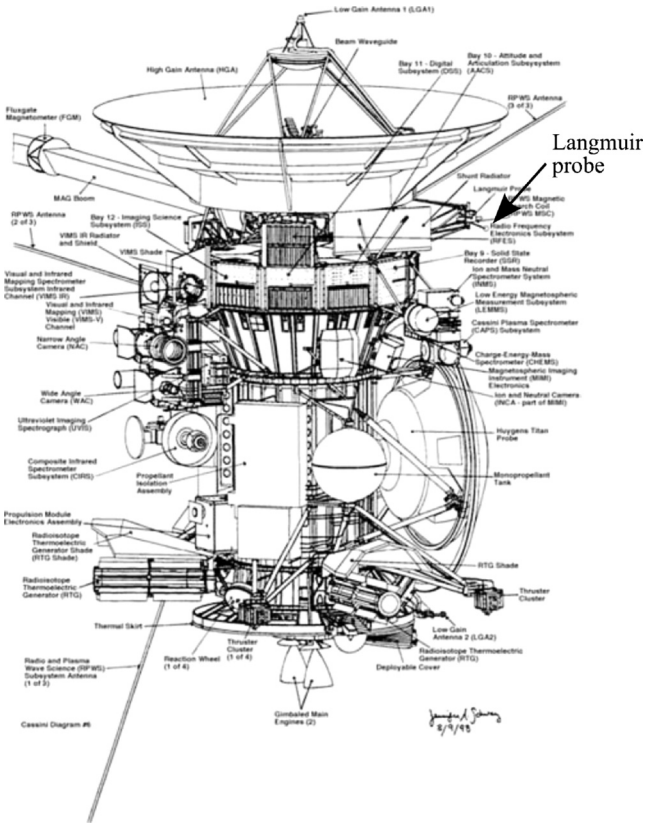

FIG. 8. The geometry of Cassini is complicated and determining how the photoelectron production from the many different parts depends on the direction of the Sun is outside the scope of the present work. This diagram is also a reminder that the spherically symmetric model used here should be expected to give qualitative results, rather than quantitative (image adapted from Ref. 8).

tential. We need to consider what populations, other than ambient electrons, contribute to the information-carrying derivative dI/dU_{LP} of the probe current (see Fig. 7). (1) There is a directed flow of ions due to the spacecraft motion (15–20 km/s) and the corotation of the plasma with Saturn (~40 km/s). This population gives a current that varies very little with probe bias, and therefore should contribute only marginally to the derivative. (2) There is a photoemission current from the probe, known to be of the order of 400 pA,[7] which flows only when the probe is negatively charged or slightly positive. This current should therefore give a peak in the derivative at and closely above the potential U_1, with a width of a few eV, corresponding to the typical photoelectron energy $k_B T_{ph}/e$. (3) The probe might also collect photoelectrons from sunlit parts of the spacecraft. Here, it is useful to introduce the concept of a *photoelectron footpoint* (see Fig. 7). This is the area from which photoelectrons would hit an unbiased probe, i.e., at $U_{LP} = U_1$. The current from this area is efficiently suppressed only when $U_{LP} < U_{SC} - k_B T_{ph}/e$. This current grows with increasing probe potential in the whole range up to $U_{LP} = U_1$, giving a positive contribution to dI/dU_{LP}. The shape of dI/dU_{LP} below and around U_1 therefore depends crucially on spacecraft geometry. Above U_1, the probe attracts and collects also electrons from an increasing area outside the photoelectron footpoint. A local structure that is well exposed to sunlight, for example, a part of the probe shaft, could give a large contribution to dI/dU_{LP}. If such a structure is inside the photoelectron footpoint, this contribution is found below U_1 but if it is outside, the contribution is found somewhere above U_1. Figure 8 shows that the geometry is very complicated and predicting the photoelectron contribution would be difficult.

In summary, the ion current would not show up significantly on the measured dI/dU_{LP} curve, but we can expect a feature just above U_1 due to photoelectrons leaving the probe and also spacecraft photoelectron features with an unknown shape that depends on the geometry and the angle of illumination.

For the spacecraft floating potential we use

$$U_{SC} - U_{pl} \approx -2.5 \frac{k_B T_e}{e}. \tag{8}$$

This corresponds to $K_{float} = 2.5$. This value is based on a particle-in-cell (PIC) simulation using a more realistic Cassini spacecraft geometry by Nilsson[9] and holds approximately in a range of plasma densities $10^6\ m^{-3} < n_{e0} < 10^8\ m^{-3}$ and temperatures $0.1\ eV < k_B T_e < 10\ eV$. It also agrees with a calculation of our own of the floating potential of the Cassini Langmuir probe in the streaming-plasma environment of Saturn's magnetosphere. We regard this value to be uncertain with about 20%, and sufficiently accurate for the present study.

We also need to choose an effective spacecraft radius r_{SC} for our probe-in-sheath model, such that the probe is at a correct depth, i.e., potential U_1, with Eq. (8) used for the spacecraft floating potential. Each curve in Fig. 9(a) represents a specific ratio ℓ_{boom}/r_{LP}. The thick (red) curve corresponds to the real Cassini spacecraft values $r_{LP} = 25$ mm and $\ell_{boom} = 1.5$ m. We choose $r_{SC} = 8$ m, for which the potential U_1 in Fig. 9(a) agrees with the PIC simulations of Nilsson,[9]

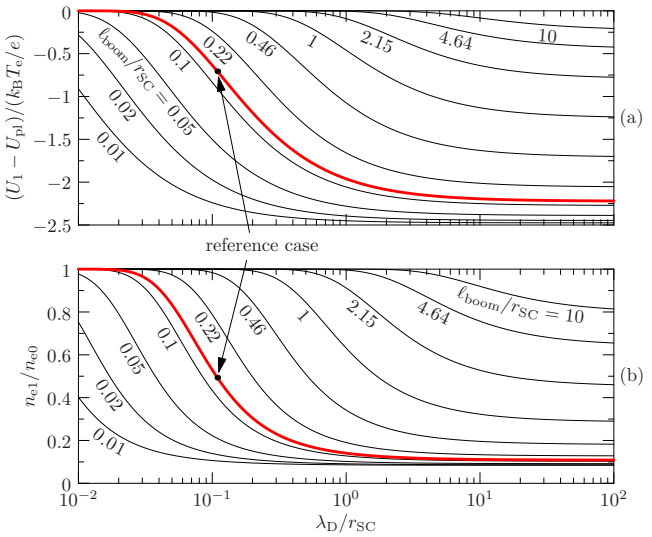

FIG. 9. (Color online) A set of curves for assessing the influence of probe-in-sheath effects on a given spacecraft, in a situation where the plasma parameters are approximately known. (a) The potential U_1, as a function of normalized parameters λ_D/r_{SC} and ℓ_{boom}/r_{SC}, assuming $K_{float}=2.5$. (b) The resulting reduction of electron density by a Boltzmann factor at the probe position. The dots on the thick curves mark the Cassini standard case of Table I. In this parameter regime, the probe-in-sheath effects are clearly very sensitive also to variations in the plasma density and temperature, through the Debye length λ_D. Curve fitting with the probe-in-sheath model must therefore include a separate calculation of U_M for each tried combination of n_e and T_e.

using the same plasma parameters. This radius is clearly larger than the actual size of Cassini, but this is expected due to the difference in shape between the actual spacecraft and our spherical model. As seen in Fig. 8, the Langmuir probe does not reside outside a spherical, or even convex, surface, but is to some extent surrounded by the disc antenna and other parts. The spacecraft potential will therefore have a greater influence over the potential at the probe position than in a model with a spherical spacecraft of similar size. To compensate for this, the spacecraft radius in the model needs to be larger. With such fixed r_{LP}, ℓ_{boom}, and r_{SC}, the thick (red) curve in Fig. 9(a) can be interpreted as the variation of U_1 with λ_D, while Fig. 9(b) shows the corresponding Boltzmann factor reduction of plasma density at the probe location. The dots on the curves show our reference case, with typical parameters from the Saturn E-ring environment. The density reduction at the probe is around 50% in the reference case, and varies considerably with λ_D, directly demonstrating the need to account for probe-in-sheath effects.

Before proceeding to the comparison between the OML and probe-in-sheath models and the data, we want to make a comment on fudge factors. These are parameters that can be embedded in a model and adjusted at will to make it fit better. The OML equations of Eq. (1) contain no fudge factor. There is no freedom of modification except by varying the plasma parameters T_e, n_{e0}, and U_{pl}. We claim the same to be true also for our probe-in-sheath model. All extra input parameters in Eq. (7), besides T_e, n_{e0}, and U_{pl}, can in principle be determined objectively: ℓ_{boom} and r_{LP} are the real values, while K_{float} and r_{SC} can be based on separate investigations, in our case, the PIC model of the potential structure around Cassini.

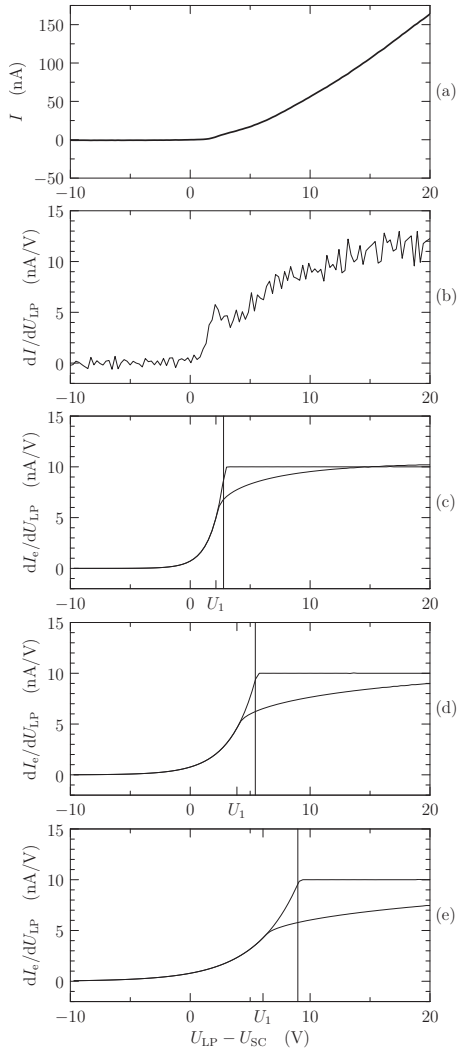

FIG. 10. A comparison between Cassini Langmuir probe data and the OML and probe-in-sheath models. (a) A measured probe sweep and (b) its derivative. We propose that the feature found where $U_{LP}-U_{SC}$ is between 2.5 and 3.5 V might be photoelectron-induced. There is no clear knee in the derivative that directly gives U_{pl} and no clear exponential part that directly gives T_e. The most useful feature is therefore the saturation level of the derivative that gives a value of the combined parameter $n_{e0}/\sqrt{T_e}=4.41\times10^5$ m$^{-3}\cdot$K$^{-1/2}$. (c) OML and probe-in-sheath model curves of dI_e/dU_{LP} with $n_{e0}=5\times10^7$ m^{-3}, $k_BT_e=1.11$ eV, and $U_{SC}-U_{pl}=-2.5k_BT_e/e$. The vertical line indicates where the probe is at the plasma potential and "U_1" where it is at the potential of its immediate surroundings. (d) The same with $n_{e0}=7\times10^7$ m^{-3} and $k_BT_e=2.17$ eV. (e) The same with $n_{e0}=9\times10^7$ m^{-3} and $k_BT_e=3.59$ eV. We consider the best fit of the six model curves to be the probe-in-sheath model in panel (d). That also corresponds to the best agreement with an independent measurement of the plasma density $n_{e0}=(6.8\pm0.2)\times10^7$ m^{-3} by the upper hybrid probe. We regard this good agreement rather fortuitous, considering the rough approximations we have made here.

Figures 10(a) and 10(b) show the current and its derivative, from the sweep by the Langmuir probe on Cassini, as a function of the applied bias voltage relative to the spacecraft. It has several common features. In particular, a "bump" on the dI/dU_{LP} curve around 2–4 V bias is found on many probe sweeps from this region. The integrated area under this bump is generally too large for it to be due to the ~400 pA photoemission current from the probe itself. A second feature found on all sweeps is a saturation in the dI/dU_{LP} curve, often followed by a small decrease at high positive potential.

The saturation level varies with distance from the ring plane. Both in the OML model of Eq. (1) and in our probe-in-sheath model of Eq. (7), such a saturation level locks the combined parameter $n_{e0}/\sqrt{T_e}$ and since $U_{SC}-U_{pl}$ is determined by T_e through Eq. (8), this leaves only one degree of freedom in fixating the triple $(U_{SC}-U_{pl}, n_{e0}, T_e)$. Consequently, a value of one of these three parameters determines the other two.

Each of Figs. 10(c)–10(e) show one OML and one probe-in-sheath model curve for a combination of electron temperature and plasma density that is consistent with the saturation plateau of the measured sweep. Out of these six curves, we regard the best fit (disregarding the proposed photoemission feature) to be obtained by the probe-in-sheath model and for the combination $n_{e0}=7\times10^7$ m^{-3} and $k_BT_e=2.2$ eV. This is also the reference case used earlier in this paper. Separate support for this to be the correct combination is found in the independent plasma density obtained from the upper hybrid frequency $f_{uh}=(f_{pe}^2+f_{ce}^2)^{1/2}$, $n_{e0}=(6.8\pm0.2)\times10^7$ m^{-3}. We therefore tentatively interpret the data in Figs. 10(a) and 10(b) as influenced by probe-in-sheath effects an photoemitted electrons from the spacecraft. Region I, where it might have been possible to estimate T_e from the exponential OML part (see, for example, Fig. 6), is corrupted by photoemission and in region II, a straightforward OML interpretation would be corrupted by probe-in-sheath effects.

VI. SUMMARY AND DISCUSSION

The main finding in this work is qualitative, rather than quantitative: the existence of the transition region, in which the probe characteristic is likely to depart from usual OML theory in respects that has a detrimental effect on the process of extracting plasma parameters from measured $I(U_{LP})$ by usual techniques: (1) the ambient plasma potential U_{pl} falls here, but there is no obvious knee or other feature to identify it, (2) there is in the transition region no exponential part of $I_e(U_{LP})$ that can be used to obtain T_e, instead (3) the curve shape depends on the probe size in a way that, for reliable quantitative evaluation, needs to be separated from the dependencies on n_{e0} and T_e. For more accurate results, models are needed that include a realistic, self-consistently obtained potential structure around the spacecraft, how it is modified by a variable probe potential, and better understanding (probably through particle simulations) of the electron collection to the probe in such a potential structure.

ACKNOWLEDGMENTS

H.G. is supported by the Belgian Science Policy Office through the Solar-Terrestrial Centre of Excellence.

[1] J. E. Allen, Phys. Scr. **45**, 497 (1992).
[2] P. M. Chung, L. Talbot, and K. J. Touryan, *Electric Probes in Stationary and Flowing Plasmas* (Springer, New York, 1965).
[3] V. I. Demidov, S. V. Ratynskaia, and K. Rypdal, Rev. Sci. Instrum. **73**, 3409 (2002).
[4] D. A. Gurnett, W. S. Kurth, D. L. Kirchner, G. B. Hospodarsky, T. F. Averkamp, P. Zarka, A. Lecacheux, R. Manning, A. Roux, P. Canu, N. Cornilleau-Wehrlin, P. Galopeau, A. Meyer, R. Boström, G. Gustafsson, J.-E. Wahlund, L. Åhlen, H. O. Rucker, H. P. Ladreiter, W. Macher, L. J. C. Woolliscroft, H. Alleyne, M. L. Kaiser, M. D. Desch, W. M. Farrell, C. C. Harvey, P. Louarn, P. J. Kellogg, K. Goetz, and A. Pedersen, Space Sci. Rev. **114**, 395 (2005).
[5] J.-E. Wahlund, M. André, A. I. E. Eriksson, M. Lundberg, M. W. Morooka, M. Shafiq, T. F. Averkamp, D. A. Gurnett, G. B. Hospodarsky, W. S. Kurth, K. S. Jacobsen, A. Pedersen, W. Farrell, S. Ratynskaia, and N. Piskunov, Planet. Space Sci. **57**, 1795 (2009).
[6] D. R. Nicholson, *Introduction to Plasma Theory* (Krieger, Florida, 1992).
[7] M. Holmberg (Exam work report, Uppsala University, Uppsala, Sweden, 2010).
[8] D. L. Matson, L. J. Spilker, and J.-P. Lebreton, Space Sci. Rev. **104**, 1 (2002).
[9] T. Nilsson, "Modelling of Cassini Langmuir probe measurements," M.S. thesis, Swedish Institute of Physics, 2009.